Research Article – Vol. 01, Issue 04, No. 03

Advanced in Engineering and Intelligence Systems

Journal Web Page: https://aeis.bilijipub.com

Construction of Mechanical Earth Model (MEM) to determine the goemechanical properties of reservouirs: a case study

Annabelle Graham [1], Emma Scott [2], William Ward [2,*]

[1] *Swinburne Univ Technol, Fac Sci Engn & Technol, Melbourne, Vic 3122, Australia*
[2] *RMIT Univ, Melbourne, Australia*

Highlights

- *The oil and gas sector has taken the mechanical earth model (MEM) into consideration*
- *MEM is a potent instrument for hydraulic fracturing and drilling design optimization*
- *The location of the least horizontal stress is where the largest tangential stress is found*
- *Tensile failure occurs in the direction of maximum horizontal stress*

Article Info

Received: 29 October 2022
Received in revised: 25 December 2022
Accepted: 25 December 2022
Available online: 01 January 2023

Keywords

mechanical earth model (MEM),
shear failure,
tensile failure,
stress regime

Abstract

The mechanical earth model (MEM) has recently been considered in the oil and gas industry due to its importance in predicting the safe and stable range of drilling mud, better understanding the effective parameters in wellbore instability, safe drilling and reduce exorbitant costs on the industry and understanding the geomechanical properties of the reservoir. The MEM includes a logical set of information related to geology, stress field, mechanical properties of rock (elastic modulus and rock failure properties) and pore pressure which can be employed as a tool to quickly update information for use in drilling and reservoir management. In this paper, a MEM was constructed using well logging data for a well in one of the oil-fields as a case study and calibrated using laboratory results and drilling reports. According to the results obtained from the minimum horizontal stress values and the maximum horizontal stress range, as well as the occurrence of tensile failures in the wellbore, it was found that the stress regime prevailing in the study field is a strike-slip fault regime. The results also show that shear failure occurs in the direction of minimum horizontal stress and tensile failure occurs in the direction of maximum horizontal stress.

1. Introduction

The use of MEM is completely established in the oil and gas industry. Several studies have been conducted due to the importance of the MEM from drilling to production in a well or oil-field, which indicates the efficiency of the MEM in both technical and economic aspects.

In the early 1990s, a challenge arose in the development of earth studies based on the analysis of geomechanical parameters in the Quiziana field in Colombia. The severity of the problems related to well instability indicated that conventional methods were not able to solve the events that occurred. Therefore, a team consisting of several large companies including geologists, geomechanical engineers, and software specialists began collecting geomechanical data. The instability of the well was still a persistent problem while completing this information and building the base model. This experience was the first step in the construction and development of the MEM [1, 2].

Using a MEM, Lee et al. [3] compared the costs and extent of risk changes during drilling in the Camisi gas-field in Peru. They found that the amount of risk and cost was greatly reduced by applying MEM, because it enabled the drilling team to recognize the hazards and challenges before and during drilling. Afsary et al. [4,5] found in their research that: 1) In deep water drilling in the Gulf of Mexico, a suitable estimate of the pore pressure in the depths of the formations was obtained with the help of

* Corresponding author : William Ward
Email: W.w01614314@gmail.com

MEM and momentary management of drilling mud pressure. 2) In one of the Canadian wells, the construction of a MEM caused the drilling of the first long horizontal well directly in the Hibernina field with a length of 6.8 km to be successfully performed. 3) The construction of a MEM for drilling and exploration well in the US folding and faulting led to an accurate estimate of the reservoir rock mechanics information in the early days of drilling and this information led to drilling in that area performed with high speed and minimal cost and risk. During their research, Richard Plumb et al. [1] discussed the reasons for the importance of the MEM, the necessity of geomechanical studies in the oil industry, as well as the uses and results obtained from the construction and presentation of the MEM. The results of this study show the efficiency of these models in improving the design, construction and operation of an oil well. Razi et al. [6] conducted studies in 2002 on the use of MEM in optimizing the drilling of the Asmari Formation in Mansouri oil-field. Saber Hosseini et al. [7] conducted their study to construct a finite element numerical model of the well and to analyze and optimize the drilling mud pressure in the horizontal well and in the strike-slip stress regime (which includes most of the fields in the Zagros Basin). In addition to the above, regarding the estimation of fracture pressure, Saber Hosseini et al. [8] build the first three-dimensional model of coupling fluid flow and rock mechanics to fully simulate the process of creating and expanding hydraulic fracturing to calculate formation pressure and analyze in-situ stresses and pore pressures on fracture pressure and fracture geometry including its length, width and height.

With the combination of MEM and discrete fracture networks (DFN), a more representative reservoir characterization can be achieved [9]. Moreover, in hydraulic fracturing modeling, rock mechanical properties such as Young's modulus, Poisson's ratio, and brittleness, which can be derived from MEM, are essential [10].

Geostatistical algorithms were applied by Ebrahimi et al. [11] to create a 3D MEM of the system. To account for geomechanical uncertainty, the authors created several MEM realizations. To propagate 1D MEMs onto 3D MEMs, first, they built 1D MEMs using the available data at well locations, and then they used ordinary Kriging. Motahari et al. [12] also developed a MEM and calibrated it using the required information to estimate the safe mud-weight windows.

In this project, the MEM in Ilam and Sarvak structures was made using data from petrophysical plots as well as core data and uniaxial and triaxial tests for well A in Hengam oil-field, which is located in the Persian Gulf Basin. A series of core data and tests obtained from them conducted in one of the fields adjacent to the Hengam oil-field and Sarvak formation have been used to calibrate the petrophysical plots since the necessary laboratory tests were not conducted in this well.

2. Introducing the studied oil-field

Hengam oil-field in the Persian Gulf is located 40 km south of Qeshm Island and 30 km south of Hengam Island in the Strait of Hormuz. Hengam oil-field is a joint field between Iran and Oman with a water depth of 70 m. This field is located on the top of Ilam Formation and its direction is north to south, which corresponds to the main direction of Oman Mountain. Hengam oil-field was discovered in 1975 by drilling well number 1. This well was tested in Ilam and Sarvak constructions and production started from this well after perforation. Well A of Hengam oil-field has been drilled 1400 m north of well number 1 of this field and its main reserveoirs include Ilam, Sarvak, Darian and Fahlian formations. Hengam oil-field belongs to the active salt dome of Hormuz geograpgically like many fields in the Persian Gulf basin, which dates back to the Precambrian era [13].

Well A from Hengam oil-field is an appraisal well that has been drilled to obtain more geological and reservoir information in this field before the start of Hengam oil-field development. Preliminary studies also show that Bangestan group (Ilam and Saruk formations) are the main hydrocarbon reservoirs.

The main formations of Ilam and Sarvak often consist of limestone lithologically with a small inner layer of shale. Illite is considered as the main clay in these formations. Limestone is dense in these formations and has poor initial porosity. Gurpi Formation has two parts in Hengam oil-field, which Gurpi-Shale section in Hengam oil-field plays the role of caprock for Ilam and Sarvak formations.

The main composition of Ilam Formation with a thickness of approximately 20 m based on petrophysical data is limestone and the percentage of porosity in this formation is between 0 to 15 and also has an average net porosity of 9.78%, a water saturation percentage of 8.26% and an average permeability of 13.16 mD. Sarvak Formation consists of three parts: Upper Sarvak, Middle Sarvak and Lower Sarvak, which mainly contain limestone. The geological structure of well A of Hengam field is shown in Figure 1. Data related to these graphs are available from a depth of 2729 to 3912 m.

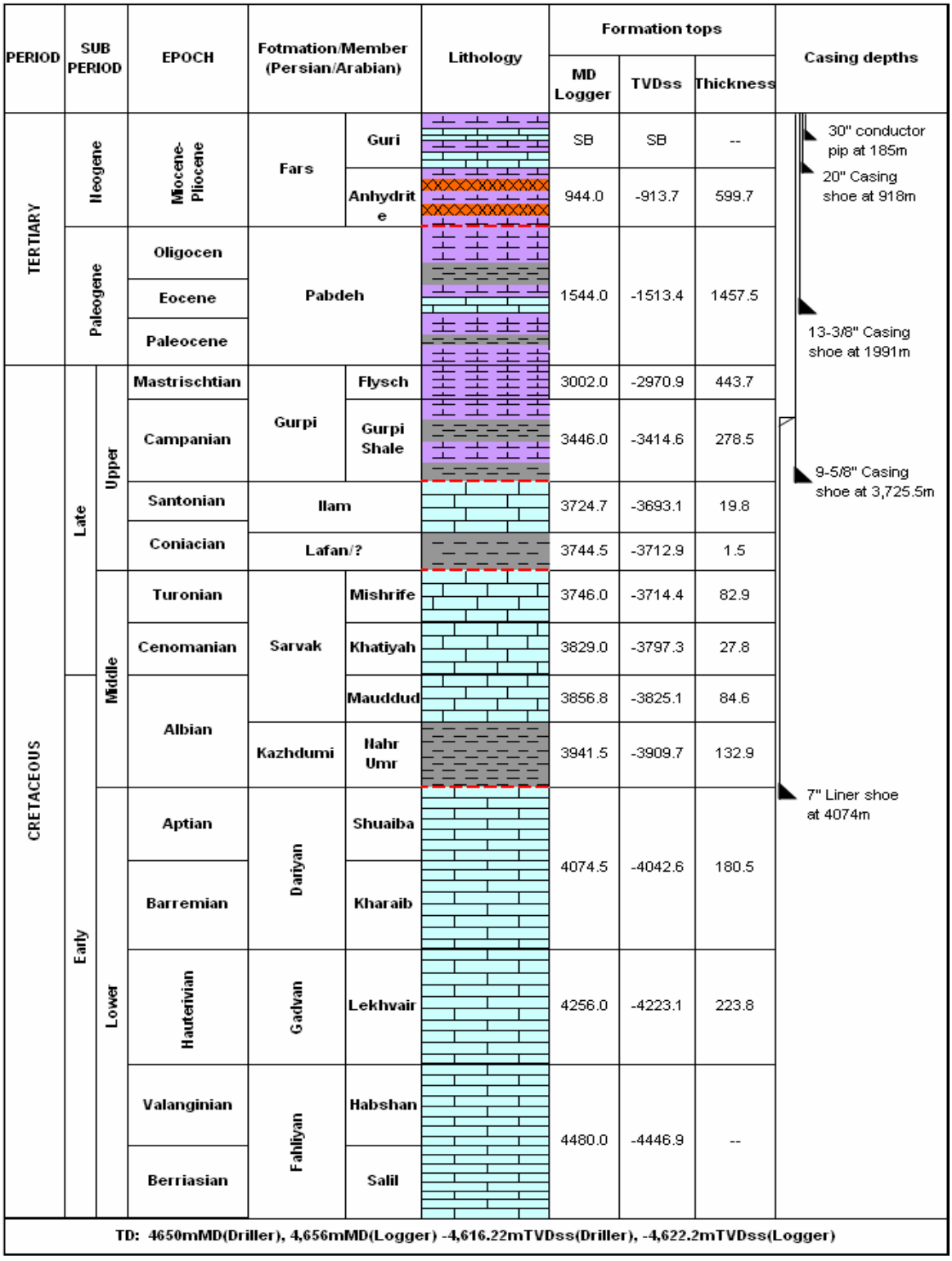

Fig. 1. Geological structure of well An in Hengam oil-field [13]

3. Construction of MEM In

3.1. *Mechanical properties of rock*

The mechanical properties of the rock are usually obtained directly by testing the cores or by means of plot measurements. Evaluation of rock strength from wireline logs is important in calculating wellbore stability, sand control and hydraulic fracturing control. The most common method used to determine elastic parameters is Dipole Sonic Images (DSI) [14]. We obtained data related to

pressure and shear waves in well A in the Hengam oil-field through the DSI and the values of elastic modulus were calculated using this informations.

3-1-1- Elastic modulus

In this study, the dynamic Young's modulus with compression and shear wave velocities was calculated from the following relation [15]:

$$E_d = \rho_b V_s^2 \left| \frac{3V_p^2 - 4V_s^2}{V_p^2 - V_s^2} \right| \quad (1)$$

Figure 2 shows the values of the dynamic Young's modulus in terms of depth in well A of the Hengam oil-field.

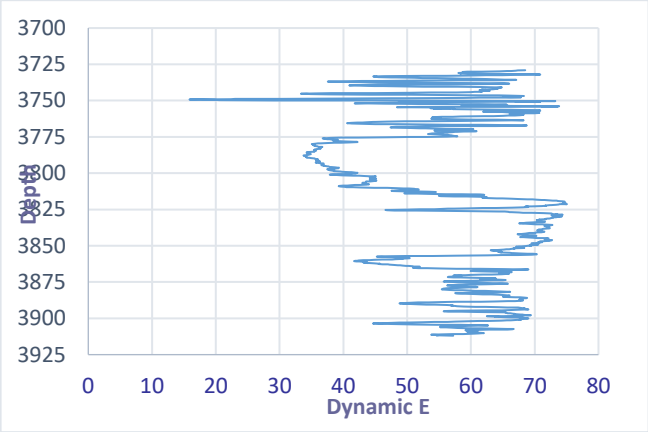

Fig. 2. Dynamic Young's modulus changes in terms of depth in well A of Hengam field.

The dynamic Poisson's ratio can also be calculated from the following equation [15]:

$$\upsilon_d = 0.5 \left| \frac{V_p^2 - 2V_s^2}{V_p^2 - V_s^2} \right| \quad (2)$$

Figure 3 shows a diagram of the dynamic Poisson's ratio in terms of depth.

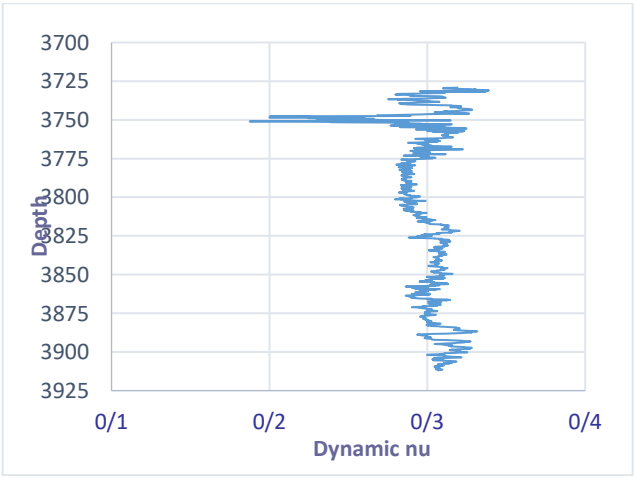

Fig. 3. Changes in dynamic Poisson's ratio in terms of depth in well A of Hengam oil-field

The data obtained from the core samples in these experiments were used to calibrate the data obtained from the plots and to obtain the static values of the elastic modulus. The values of Young's modulus, Poisson's ratio, internal friction angle and cohesion in the cores were measured.

The following equation was obtained for well A of Hengam oil- field using the available data, between the dynamic and static Young's modulus:

$$E_s = 0.5301E_d + 0.6104 \quad (3)$$

Figure 4 shows the static and dynamic Young's modulus data with the above developed equation.

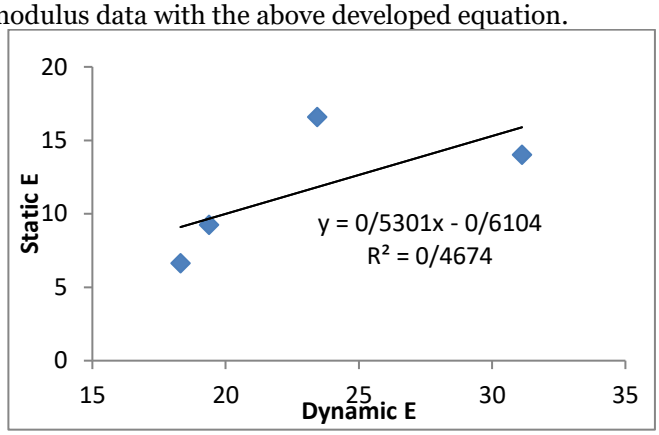

Fig. 4. Relationship between static and dynamic Young's modulus in well A of Hengam oil-field.

The data related to the cores were used as in Young's modulus in order to obtain the relationship between static and dynamic Poisson's ratio, which are shown in Figure 5. The following equation was obtained for well A of Hengam oil-field, between dynamic and static Poisson's ratio:

$$\upsilon_s = 0.6398\upsilon_p - 0.023 \quad (4)$$

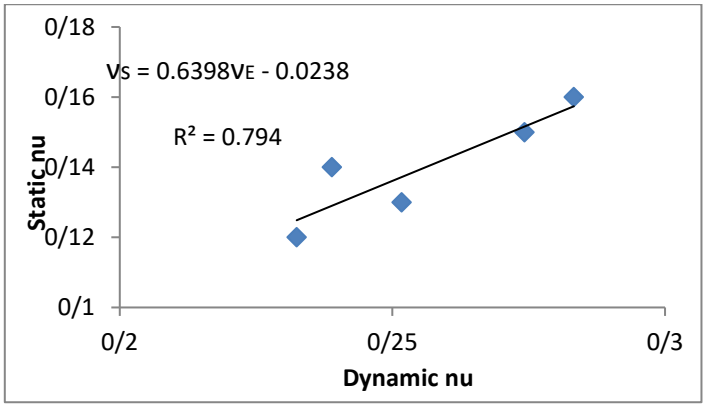

Fig. 5. Relationship between static and dynamic Poisson's ratio in well A of Hengam field.

Figures 6 and 7 show the differences between the static and dynamic Young's modulus and the differences between the static and dynamic Poisson's ratio, respectively.

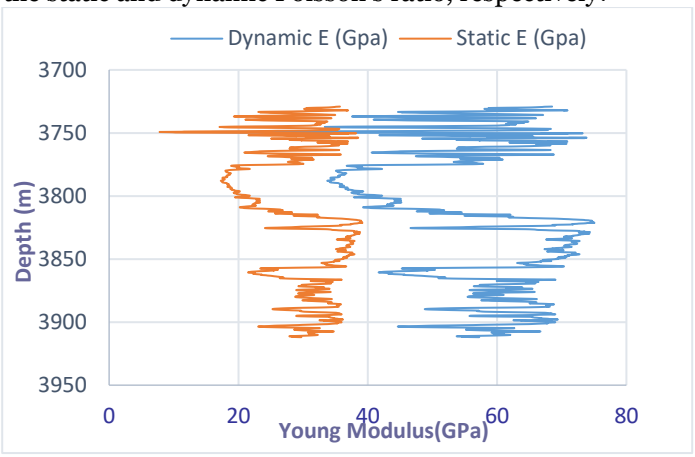

Fig. 6. Scattering of static and dynamic values of Young's modulus in terms of depth.

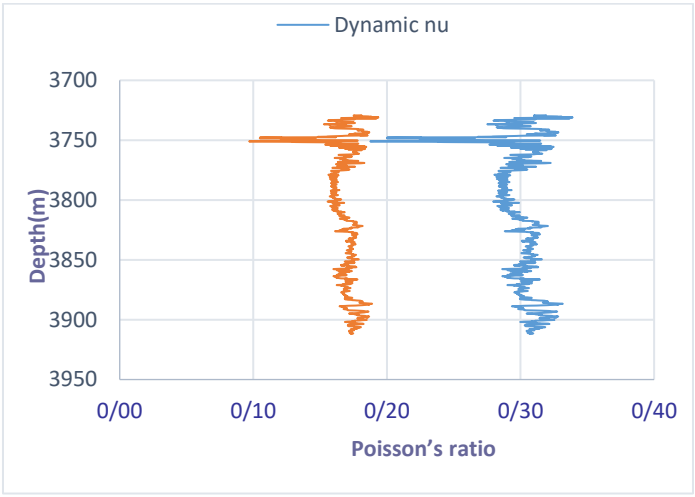

Fig. 7. Scattering of static and dynamic Poisson's ratio in terms of depth.

Because the behavior of the rock in calculations and simulations is assumed to be elastic, shear modulus (G), bulk modulus (K) and lame coefficient (λ) can be calculated by having a Poisson's ratio and a static Young's modulus. The relationships required to obtain these coefficients are listed in Table 1.

Table 1. Relationships between different static modulus [16]

$E = eK(1-2v)$	$K = \lambda\frac{1+v}{3v}$	$2v = \frac{\lambda}{\lambda+G}$
$E = 2G(1+v)$	$K = \frac{2}{3}G\frac{1+v}{1-2v}$	$1-2v = \frac{G}{\lambda+G}$
$E = \frac{9KG}{3K+G}$	$K = \lambda + \frac{2}{3}G$	$2(1-v) = \frac{\lambda+2G}{\lambda+G}$
$E = G\frac{3\lambda+2G}{\lambda+G}$	$K = \frac{GE}{9G-3E}$	$2(1+v) = \frac{3\lambda+2G}{\lambda+G}$
$E = \frac{\lambda}{v}(1+v)(1-2v)$	$\frac{\lambda}{G} = \frac{2v}{1-2v}$	$2(2-v) = \frac{3\lambda+4G}{\lambda+G}$

3-1-2- Calculation of rock strength

In this paper, the results of tests performed on a series of samples in one of the fields adjacent to the Hengam oil-field were used to obtain the value of uniaxial compressive strength. After examining the laboratory data and considering the type of the studied formations, which was mainly limestone, no special relationship was observed between the data parameters and uniaxial compressive strength of the rock and the best relationship is the relationship between uniaxial compressive strength and static Young's modulus.

The relation based on the static Young's modulus for uniaxial compressive strength can be obtained using the results of laboratory tests:

$$UCS = 7.072\ E_s^{0.817} \quad (5)$$

Figure 8 shows the relationship between uniaxial compressive strength and static Young's modulus.

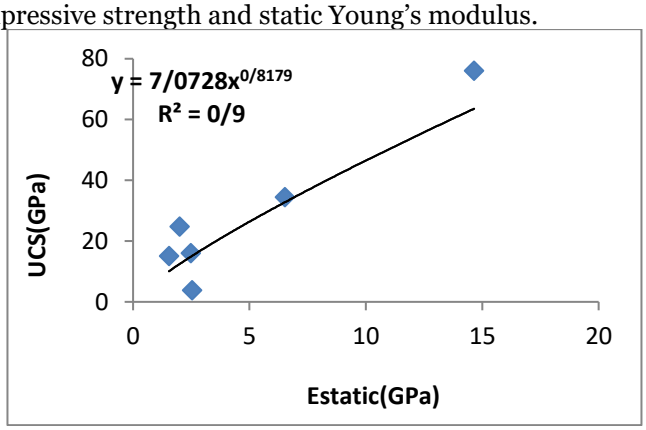

Fig. 8. Relationship between uniaxial compressive strength and static Young's modulus.

The value of uniaxial compressive strength can be obtained for different depths using the equation 5. Figure 9 shows the changes in uniaxial compressive strength in the well A.

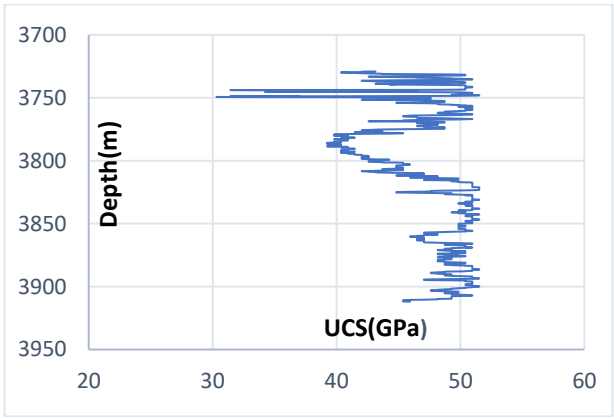

Fig. 9. Uniaxial compressive strength changes in depth for well A of Hengam oil-field.

Regarding the tensile strength of the rock, which is denoted by the symbol T_o, no information is available about the value of this rock strength in this field, so this parameter was considered equal to 1/10 of the compressive strength of the rock, which is a common value in the work done [17].

3-1-3- Internal friction angle

In this reseach, a porosity-based equation for the internal friction angle was obtained like the elastic modulus, using the data available from the tests performed on the cores for the internal friction angle:

$$\varphi = 51.527 - 55.82\phi \quad (6)$$

Figure 10 shows the relationship between porosity and internal friction angle. Using the obtained equation, it is possible to show the changes in the internal friction angle in terms of depth (Figure 11).

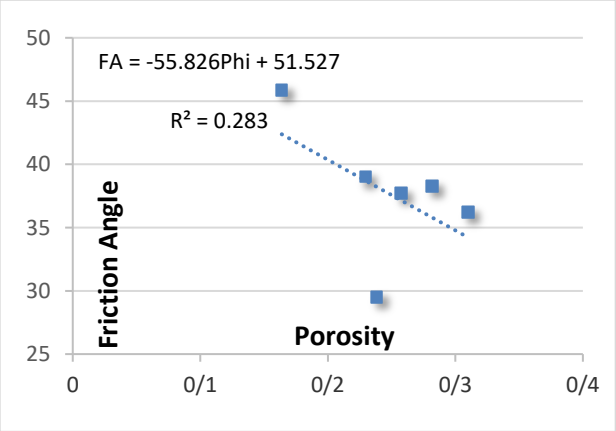

Fig. 10. Relationship between porosity and internal friction angle for well A of Hengam oil-field

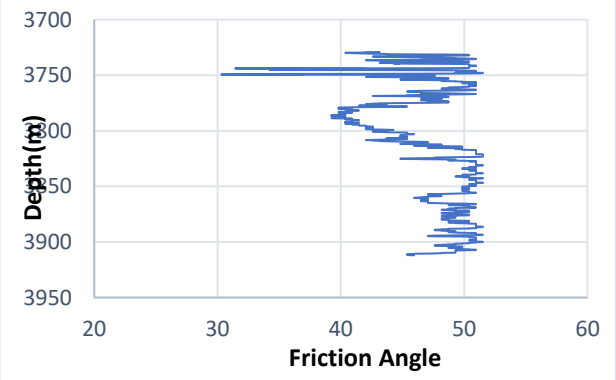

Fig. 11. Changes in the internal friction angle in terms of depth in well A of Hengam oil- field.

3.2 Pore pressure

Modular Dynamic tests (MDT) were performed in well A of Hengam oil-field. Therefore, pore pressure can be obtained for different depths using these tests. Also, equations in terms of depth for hydrostatic pressure and pore pressure can be obtained using the data we have available. As can be seen in Figure 12, the pressure at these depths is greater than the hydrostatic pressure and therefore will be of the abnormal pressure type. The equation for hydrostatic pressure is as follows:

$$P_{Hyd} = 0.01D + 3 \times 10^{-11} \quad (7)$$

We also have for pore pressure:

$$P_P = 0.0053D + 28.161 \quad (8)$$

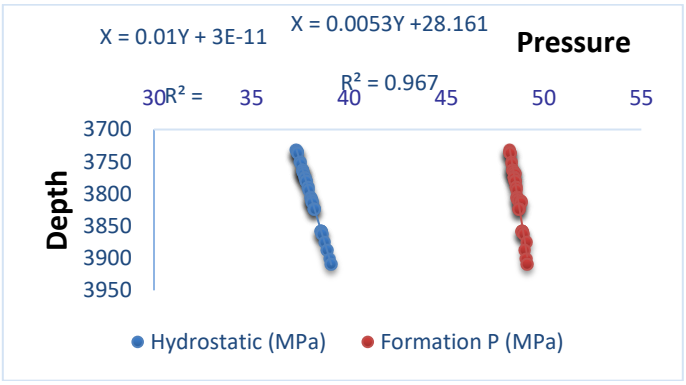

Fig. 12. Changes in hydrostatic and pore pressure in terms of depth in well A of Hengam oil-field.

3.3 Overburden in-situ stress

Checking the on-site stress field in a well or reservoir consists of several parts. In the first step, the magnitude of the vertical stress or overburden stress must be calculated. In the next step, the directions of the horizontal stresses must be measured. Finally, the magnitude of the horizontal stresses must be calculated. These steps were performed for the Hengam well A in this section and the stress field including the value and directions of in-situ stresses were measured.

The density log is integrated from the surface to the final depth to measure the overburden stress [17]:

$$\sigma_v = \int_0^z \rho_b(z) g dz \quad (9)$$

Cosidering that the density graph is only available in the reservoir of this well, the existing log data were extrapolated and spread to the earth surface [18]. For this purpose, the following relationship was used [17, 19]:

$$\rho_b = \rho_{sur} + A_0(TVD - WD - AG)^{\alpha} \quad (10)$$

In this relation, ρb is the total density, ρ_{sur} is earth-surface density, TVD is the vertical depth, WD is the sea water heigh, AG is the sea water heigh, α and A_0 are the extrapolation parameters. The results of this extrapolation are shown in Figure 13. The values of 0.14 and 0.296 were obtained for the parameters A_0 andα, respectively. The density data were numerically integrated to obtain the overburden stress at different depths from the earth surface to the final well drilling depth. These changes are shown in Figure 14.

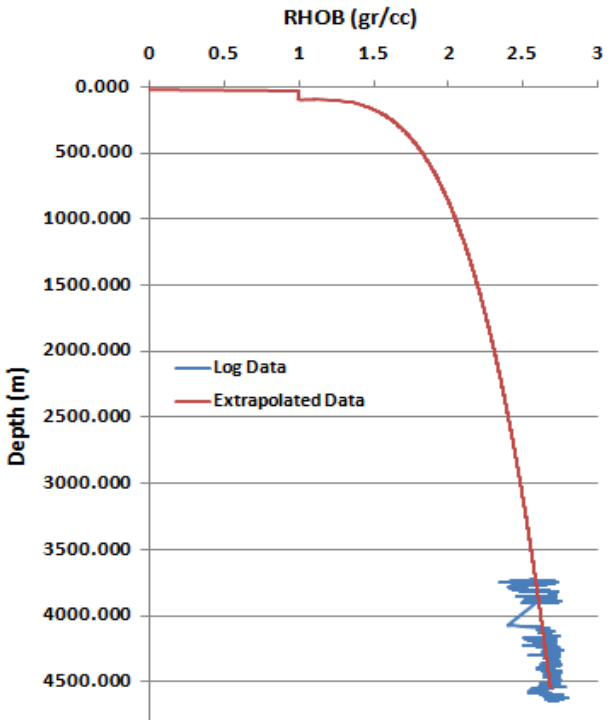

Fig. 13. Density changes in depth in well A.

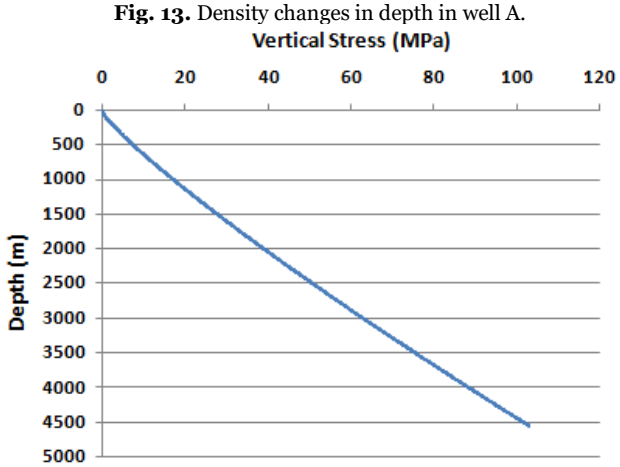

Fig. 14. Overburden stress changes in depth in well A.

3-4- Horizontal in-situ stresses

3-4-1 Directions of horizontal in-situ stresses

Information about FMI is available about different wells of the Hengam oil-field. The four tensile failures observed in the FMI in well A are shown in Figure 15. Tensile failure is seen as two narrow dark areas in the FMI image that are 180 degrees apart. The reason for the dark view of this area is the drilling fluid that fills the gap and is seen as dark due to its low electrical resistance. As can be seen in this image, the direction of tensile failures, which is the direction of maximum horizontal in-situ stress, is in the northwest-southeast direction.

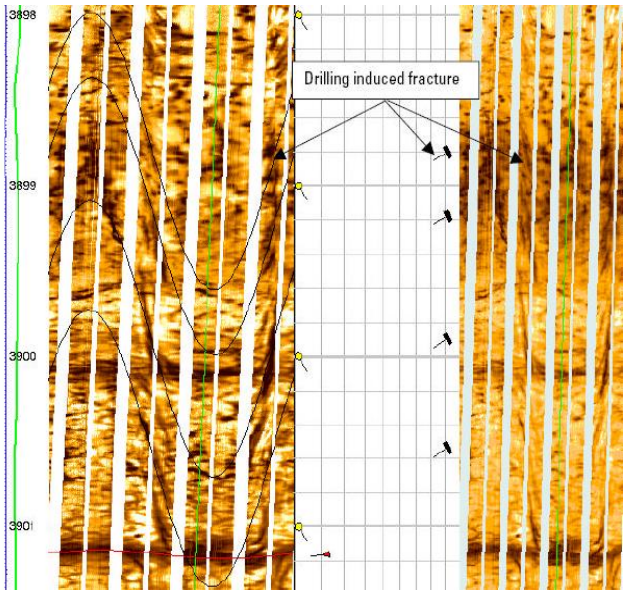

Fig. 15. FMI log, four tensile failures in well A during drilling

3-4-2 Minimum horizontal in-situ stress

In well A of Hengam, only information about the three Formation Strength Tests (FIT) is available. In this test, the mud pressure is less than the least horizontal in-situ stress. In this way, the available data from other wells were used to make a more accurate guess on the minimum horizontal in-situ stress. Several leak-off tests have been performed on the wells around Hengam A, but they are all at a certain depth. Information is also available on the several mud losses in the well number 3. The data used to estimate the minimum horizontal in-situ stress size are shown in Figure 16. To obtain an estimate of the magnitude of the minimum horizontal in-situ stress in terms of depth, a line parallel to the line passing from the strength data of the formation test data was used, which includes all the events observed during drilling and tests. As can be seen, this line is the upper limit of leak-off pressure and a loss that occurred in well 3.

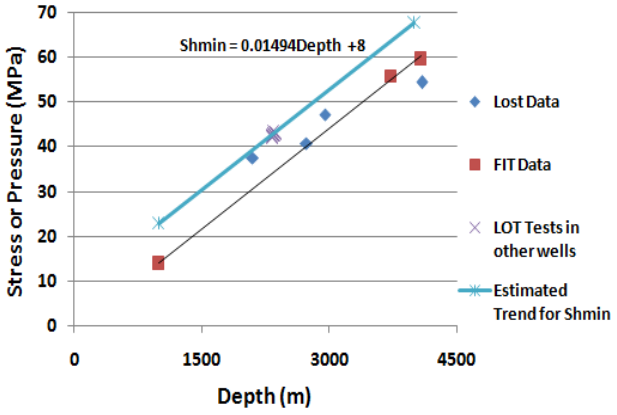

Fig. 16. Information about formation strength test, leakoff test and mud loss in different wells of Hengam oil-field.

3-4-3 Maximum horizontal in-situ stress

The magnitude of maximum horizontal in-situ stress was limited through the stress polygon method [17]. In this approach, the stress range is limited by several lines, each of which represents a specific phenomenon.

In this method, the ratio of the maximum effective in-situ stress to the minimum effective in-situ stress is obtained from the following equation:

$$\frac{\sigma_1}{\sigma_3} = \frac{S_1 - P_P}{S_3 - P_P} = [(1+\mu^2)^{\frac{1}{2}} + \mu]^2 \quad (11)$$

In this relation, μ is the fault friction coefficient. To use this relationship, it must be determined which of the minimum and maximum horizontal in-situ stresses and overburden stress replace S_1 and S_3. Anderson Faulting theory was used for this purpose. According to this theory, three states of stress regime occur as follows [17]:

Normal fault regime:

$$\frac{\sigma_1}{\sigma_3} = \frac{S_V - P_P}{S_{hmin} - P_P} \leq [(1+\mu^2)^{\frac{1}{2}} + \mu]^2 \quad (12)$$

Reverse fault regime:

$$\frac{\sigma_1}{\sigma_3} = \frac{S_{Hmax} - P_P}{S_V - P_P} \leq [(1+\mu^2)^{\frac{1}{2}} + \mu]^2 \quad (13)$$

Strike-slip fault regime:

$$\frac{\sigma_1}{\sigma_3} = \frac{S_{Hmax} - P_P}{S_{hmin} - P_P} \leq [(1+\mu^2)^{\frac{1}{2}} + \mu]^2 \quad (14)$$

Numbers between 0.6 and 1 have been used for the Earth's crust friction coefficient in various studies. Usually, the number 0.6 gives a good answer and it has been used in various studies [20]. According to the stress regime introduced above, three lines can be drawn. The stress polygons are plotted in graphs that show the maximum horizontal in-situ stress in terms of the minimum horizontal in-situ stress. Another line is drawn since the maximum horizontal in-situ stress cannot be less than the minimum horizontal stress. An example of a stress polygon for well A at depth 4026/82 is shown in Figure 17.

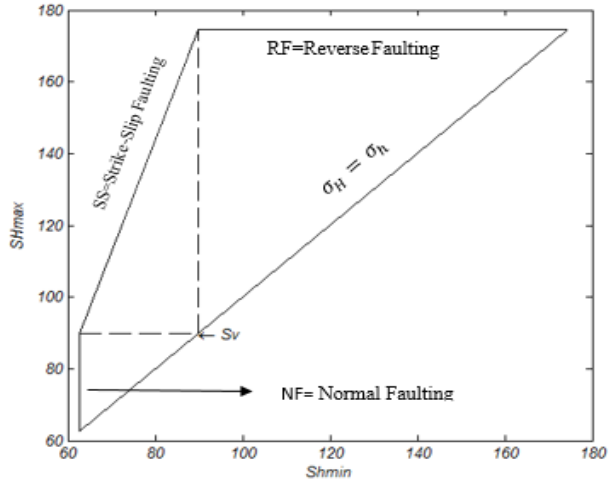

Fig. 17. General polygonal stress framework for Hangam well A at depths of 82/4026.

To limit the magnitude of horizontal in-situ stress in this project, shear and tensile failure that occurred in well number 3 were used. In Hengam well number 3, 7 shear failures and 22 tensile failures occurred. Among these failures, both shear and tensile failure have occurred at four depths. Also, at 18 depths only tensile failure occurred. These events were used to limit the magnitude of the maximum horizontal in-situ stress. For example, at a depth of 4026.82, where both tensile failure and shear failure have occurred, the maximum horizontal in-situ stress is limited to what can be seen in Figure 18. The width of the shear failures is estimated from the plots. The width of these failures varied from 30 to 60 degrees in well number 3.

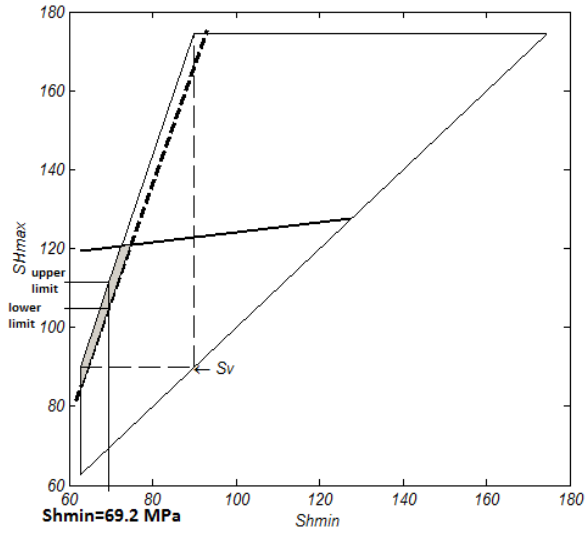

Fig. 18. Limiting maximum horizontal in-situ stress to a depth of 4026.82 in well as using tensile and shear failures occurring at this depth.

A large difference between the maximum and minimum horizontal stress values is required to induce tensile stress to occur around a vertical well. According to these three types of stress regimes, this condition occurs mainly in the strike-slip stress regime [20]. Considering this point as well as the range set for the maximum horizontal stress, it can be concluded that a strike-slip stress regime prevails in this field. Analysis was performed for all failures recorded in well 3, the results of which are related to several failures in Figure 19. The equation for the upper and lower limits of the horizontal in-situ stress is obtained if lines are crossed over the upper and lower limits of the calculations performed on the failures.

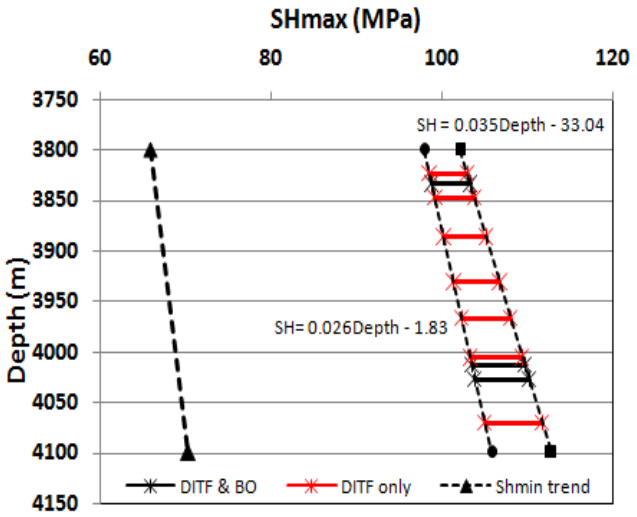

Fig. 19. Changes in the magnitude of minimum and maximum horizontal in-situ stresses at different depths.Fig. 19:

4. Conclusions

MEM is a powerful tool for optimizing drilling design and hydraulic fracturing treatment, since they integrate reservoir geology, petrophysical characterization, and in-situ geomechanical characteristics. According to the mechanical model and the values obtained for maximum and minimum horizontal stresses as well as the range specified for maximum horizontal stress in the polygonal stress method, it can be concluded that a strike-slip stress regime prevails in this field and the reason is the occurrence of tensile failures in the wellbore, which itself requires a large difference between the maximum and minimum horizontal stress, which mainly indicates the strike-slip stress regime. The method of occurrence of shear and tensile failures in the wellbore also shows that the maximum tangential stress or shear failure occurs in the direction of minimum horizontal stress, ie northeast-southwest, also, minimum tangential stress or tensile failure occurs in the direction of maximum horizontal stress, ie northwest-southeast.

REFERENCES

[1] Plumb, R., Edwards, S., Pidcock, G., Lee, D., & Stacey, B. (2000, February). The mechanical earth model concept and its application to high-risk well construction projects. In IADC/SPE Drilling Conference. OnePetro.

[2] Addis, M. A. (2017). The geology of geomechanics: petroleum geomechanical engineering in field development planning. Geological Society, London, Special Publications, 458(1), 7-29.

[3] Lee, D., Cassanelli, J. P., Frydman, M., Palacio, J., Delgado, R., & Collins, B. (2003, October). Using a dynamic Mechanical Earth Model and integrated drilling team to reduce well costs and drilling risks in San Martin Field. In SPE Annual Technical Conference and Exhibition. OnePetro.

[4] Afsari, M., Ghafoori, M., Roostaeian, M., Haghshenas, A., Ataei, A., & Masoudi, R. (2009, March). Mechanical earth model (MEM): An effective tool for borehole stability analysis and managed pressure drilling (case study). In SPE Middle East Oil and Gas Show and Conference. OnePetro.

[5] Afsari, M., Amani, M., Razmgir, S. M., Karimi, H., & Yousefi, S. (2010, June). Using drilling and logging data for developing 1d mechanical earth model for a mature oil field to predict and mitigate wellbore stability challenges. In International Oil and Gas Conference and Exhibition in China. OnePetro.

[6] Razi Perchikolaee, S., Shadizadeh, S. R., Shahryar, K., & Kazemzadeh, E. (2010). Building a precise mechanical earth model and its application in drilling operation optimization: A case study of Asmari formation in Mansuri oil field. In Society of Petroleum Engineers-International Oil and Gas Conference and Exhibition in China 2010, IOGCEC (Vol. 4, pp. 2999-3019). Society of Petroleum Engineers.

[7] Saberhosseini, S. E., Ahangari, K., & Alidoust, S. (2013). Stability analysis of a horizontal oil well in a strike-slip fault regime. Austrian Journal of Earth Sciences, 106, 30-36.

[8] Saberhosseini, S. E., Keshavarzi, R., & Ahangari, K. (2014). A new geomechanical approach to investigate the role of in-situ stresses and pore pressure on hydraulic fracture pressure profile in vertical and horizontal oil wells. Geomechanics and Engineering, 7(3), 233-246.

[9] Spence, G. H., Couples, G. D., Bevan, T. G., Aguilera, R., Cosgrove, J. W., Daniel, J. M., & Redfern, J. (2014). Advances in the study of naturally fractured hydrocarbon reservoirs: a broad integrated interdisciplinary applied topic. Geological Society, London, Special Publications, 374(1), 1-22.

[10] Liang, B., Khan, S., Puspita, S. D., Tran, T., Du, S., Blair, E., & Rives, S. (2016, August). Improving Unconventional Reservoir Factory-Model Development by an Integrated Workflow with Earth Model, Hydraulic Fracturing, Reservoir Simulation and Uncertainty Analysis. In SPE/AAPG/SEG Unconventional Resources Technology Conference. OnePetro.

[11] Ebrahimi, M. A., Ahmadi, M., & Ameri, M. J. (2020). Application of unconditional simulation methods for quantifying the uncertainties in mud window design of gas reservoirs based on 3-dimensional mechanical earth modeling. Journal of Natural Gas Science and Engineering, 76, 103186.

[12] Motahari, M., Hashemi, A., & Molaghab, A. (2022). Successful mechanical earth model construction and wellbore stability analysis using elastic and plasticity solutions, a case study. Geomechanics for Energy and the Environment, 100357.

[13] Ebadati, N. (2018). Fractures Effect in Reservoir Quality of Ilam and Sarvak Formations in Hengam Oilfield Using Imaging Logs. Journal of the Geological Society of India, 92(4), 491-497.

[14] Maleki, S., Gholami, R., Rasouli, V., Moradzadeh, A., Riabi, R. G., & Sadaghzadeh, F. (2014). Comparison of

different failure criteria in prediction of safe mud weigh window in drilling practice. Earth-Science Reviews, 136, 36-58.
[15] Peng, S., & Zhang, J. (2007). Engineering geology for underground rocks. Springer Science & Business Media.
[16] Fjar, E., Holt, R. M., Horsrud, P., & Raaen, A. M. (2008). Petroleum related rock mechanics. Elsevier.
[17] Zoback, M. D., Barton, C. A., Brudy, M., Castillo, D. A., Finkbeiner, T., Grollimund, B. R., & Wiprut, D. J. (2003). Determination of stress orientation and magnitude in deep wells. International Journal of Rock Mechanics and Mining Sciences, 40(7-8), 1049-1076.
[18] Bourgoyne, A. T., Millheim, K. K., Chenevert, M. E., & Young, F. S. (1986). Applied drilling engineering (Vol. 2, p. 514). Richardson: Society of Petroleum Engineers.
[19] Moos, D., Zoback, M. D., & Bailey, L. (2001). Feasibility study of the stability of openhole multilaterals, Cook Inlet, Alaska. SPE Drilling & Completion, 16(03), 140-145.
[20] Reynolds, S. D., Mildren, S. D., Hillis, R. R., & Meyer, J. J. (2006). Constraining stress magnitudes using petroleum exploration data in the Cooper–Eromanga Basins, Australia. Tectonophysics, 415(1-4), 123-140.